Available online at www.sciencedirect.com
SCIENCE DIRECT®
Journal of Power Sources 135 (2004) 52–61
JOURNAL OF POWER SOURCES
www.elsevier.com/locate/jpowsour

# Development of spinel forming alloys with improved electronic conductivity for MCFC applications

I. Parezanović*, E. Strauch, M. Spiegel

*Department of Interface Chemistry and Surface Engineering, Max-Planck-Institut für Eisenforschung, Max-Planck Str. 1, 40237 Düsseldorf, Germany*

Received 15 January 2004; received in revised form 29 March 2004; accepted 17 April 2004

Available online 2 July 2004

**Abstract**

The molten carbonate fuel cells (MCFC), as an alternative power source, present one of the most promising and environmental cleanest processes. As a high temperature fuel cell, problems arise due to corrosion of the metallic current collectors and voltage drop by formation of insulating corrosion products. The aim of this work is to develop Fe–Cr stainless steels, alloyed with different amounts of Mn, Co, Si, Ni, Mo, in order to obtain an acceptable thin corrosion scale with a low electrical resistivity by spinel formation. The formation of spinel layers as corrosion products, containing multivalent elements like Mn, Co and Mo is expected to give satisfactory results. In situ conductivity measurements and corrosion tests have been performed in the presence of a (Li, K) carbonate melt at 650 °C under an oxidizing gas atmosphere (15 vol.% $CO_2$ and synthetic air) up to 5000 h. Investigations of the corrosion scales on the hot rolled alloys indicated a solubility of Co and Mn in the spinel layer, formed under the simulated MCFC conditions. Outward diffusion of Mn and Co was observed after longer reaction times. An inner oxidation zone was also measured and connection between conductivity behaviour and the composition of this layers is found.


*Keywords:* Corrosion resistance; Conductivity; Diffusion; Inner oxides

## 1. Introduction

The molten carbonate fuel cell (MCFC) is a high temperature device which uses the eutectic mixture of $Li_2CO_3/K_2CO_3$ or $Li_2CO_3/Na_2CO_3$ as electrolyte. At 650 °C working temperature transport of $O^{2-}$ occurs by migration of $CO_3^{2-}$. The cathode material is a porous nickel, which is in situ transformed to lithiated NiO whereas the anode material is a metallic nickel foam. Gas mixture of $H_2O$, $H_2$ and $CO_2$ is used on the anode side and on the cathode side a mixture of $O_2$ and $CO_2$. In an open-circuit one cell produces around 1 V and several hundred cells are connected with metallic materials (cathode current collector (CCC)) to obtain more power. The development of MCFC is progressing steadily. There are already several power plants based on MCFC and although in use, these plants still cannot reach the desirable MCFC lifetime of 40 000 h.

One of the major problems in operating the MCFC is the corrosion attack of the metallic components i.e. of the cathode current collector by the carbonate melt. This oxidation leads to metal loss and, much more important, to a significant cell voltage drop due to the formation of bad conductive oxides. Generally, the compounds in the top layer are in equilibrium with the molten carbonate and those in the inner layer with the metallic substrate. High alloyed steels with Cr content >20 wt.% are generally protected against the corrosion due to the formation of a dense chromia scale under oxidizing conditions. In the MCFC, however, soluble $K_2CrO_4$ is formed in contact with the melt and significant metal loss occurs. Additionally bad conductive $LiCrO_2$ develops on the metal/scale interface and causes a dramatic drop of voltage in a cell. In order to avoid these problems, steels with less than 20 wt.% Cr have to be developed, showing a good corrosion resistance and a tolerable resistivity of the formed oxides.

Addition of elements like Ni, Mn, Co and Mo in steels with 16–18% Cr enable the formation of corrosion protective $LiFeO_2$, $LiCoO_2$, $Li_2MnO_3$ layers in contact with the melt and inner oxide spinels based on (Fe, Ni)$Cr_2O_4$ layers with Mn, Co and Mo in solid solution. It is known, for

* Corresponding author. Tel.: +49 211 6792 334; fax: +49 211 6792 218.
*E-mail addresses:* parezanovic@mpie.die (I. Parezanović), spiegel@mpie.de (M. Spiegel).

0378-7753/$ – see front matter © 2004 Elsevier B.V. All rights reserved.
doi:10.1016/j.jpowsour.2004.04.007

example, that small amounts of Mn, Co or Cu dissolved in $LiFeO_2$ improve the electrical conductivity of $LiFeO_2$ [1]. Thanks to the spinel nonstoichiometry and n- and p-type structure defects [2], as well as the possibility of ions with a different valence to occupy the tetrahedral and the octahedral vacant sites in the crystal structure, electronic conductivity in spinels can easily occur by electron hopping between multivalent ions occupying the same crystallographic sites. Hence, conduction occurs when one type of ion is present in two different valence states occupying the same crystallographic site [3]. This is especially observed in magnetite as an inverse spinel structure $Fe^{2+}(Fe^{2+}, Fe^{3+})O_4$ which shows a nearly metallic conductivity behaviour due to electron hopping. Other oxides, for example, MnO, NiO, $Co_2O_3$ have conductivities of the order of $10^{-6}$ to $10^{-4}\,\Omega^{-1}\,cm^{-1}$, spinel-type $Co_3O_4$ has conductivity of $10^{-4}\,\Omega^{-1}\,cm^{-1}$, $NiCo_2O_4$ has $10^{-2}\,\Omega^{-1}\,cm^{-1}$, $MnCo_2O_4$ has $10^{-3}\,\Omega^{-1}\,cm^{-1}$ and the conductivity of $NiCo_2O_4$ is $0.6\,\Omega^{-1}\,cm^{-1}$ [4]. A good conductivity of spinel-type oxides is often connected with a high oxidation rates due to a good cation and anion diffusion. The main idea behind this work is to improve the electronic conductivity of an $FeCr_2O_4$ spinel with low anion and cation diffusivities by incorporating multivalent ions in the crystal structure.

For that purpose, we investigated laboratory made Fe–Cr alloys with Cr content between 17 and 18 wt.% and different amounts of alloying elements Co, Mn, Mo, Si and Ni for a better understanding of relation between the corrosion rate and the resistivity of the formed oxide layers and to develop an optimised alloy composition.

## 2. Experimental

The chemical composition of the used laboratory heats is given in Table 1. All alloys were exposed to the corrosion measurements and AC 66, V 150, V 152 and V 155 were exposed to in situ conductivity measurements.

The alloys were exposed to the carbonate mixture of 62 mol% $Li_2CO_3$ and 38 mol% $K_2CO_3$. For the corrosion measurements this carbonate mixture was melted, cooled, pulverized and mixed in a ratio of 60:40 wt.% with $LiAlO_2$, which act as a ceramic matrix. For the corrosion tests the metal samples ($1\,cm^2$) were placed on the top of a carbonate melt which was put in a crucible as shown in Fig. 1.

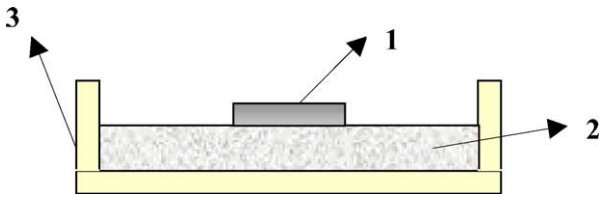


Fig. 1. Schematic of the sample arrangement for the corrosion test: (1) metallic specimen, (2) carbonate melt with $LiAlO_2$ and (3) $Al_2O_3$ crucible.

Tests were carried out in the cathodic MCFC environment (15% $CO_2$/synthetic air), with the gas flow of 1 l/h, at 650 °C for different exposure times. Microstructural examinations were done with a use of scanning electron microscopy (SEM) with energy dispersive X-ray analysis (EDX). For the electrical resistivity tests (Fig. 2) the electrical resistivity of two NiO (Li) cathodes with melt on the both sides was measured first. Afterwards, the overall resistivity of the sample arrangement was measured. From the difference between the second and the first measurement we calculated the electrical conductivity of the corroded samples. Since the resistivity of NiO cathodes changes in the first 50 h due to porosity reduction, only the measurements longer than 50 h were considered in the discussion.

If we define a resistance, $R$, as a measure of the component's opposition to the flow of electric charge, the electrical resistivity can be express as follows:

$$\rho = R\frac{S}{L} \tag{1}$$

where $L$ is the length of the material through which a current flows, $S$ the cross-sectional area and $\rho$ is the electrical resistivity of the material.

Electrical conductivity is the movement of charged particles through a material (current) in response to an electric field and is reciprocal quantity of electrical resistivity.

Table 1
Chemical composition of used materials and their designation

| Content (wt.%) | Designation | | | | | | | |
|---|---|---|---|---|---|---|---|---|
| | V 150 | V 151 | V 152 | V 153 | V 154 | V 155 | V 156 | AC 66 |
| C | 0.0354 | 0.0403 | 0.0334 | 0.334 | 0.0322 | 0.0334 | 0.0301 | – |
| Co | 5.08 | 2.98 | 4.96 | 2.96 | 3.02 | 9.75 | 9.89 | – |
| Cr | 17.8 | 17.4 | 17.6 | 17.2 | 17.1 | 17.3 | 17.3 | 27.8 |
| Mn | 2.04 | 1.98 | 12.2 | 7.13 | 7.03 | 2.00 | 2.01 | 0.487 |
| Mo | 3.01 | 3.05 | 3.03 | 3.06 | 2.91 | 4.82 | 3.11 | – |
| Ni | 12.3 | 11.6 | 2.96 | 5.65 | 5.83 | 14.1 | 14.1 | 31.2 |
| Si | 0.499 | 0.524 | 0.510 | 0.492 | 0.0226 | 0.562 | 0.516 | – |
| Nb | – | – | – | – | – | – | – | 0.85 |

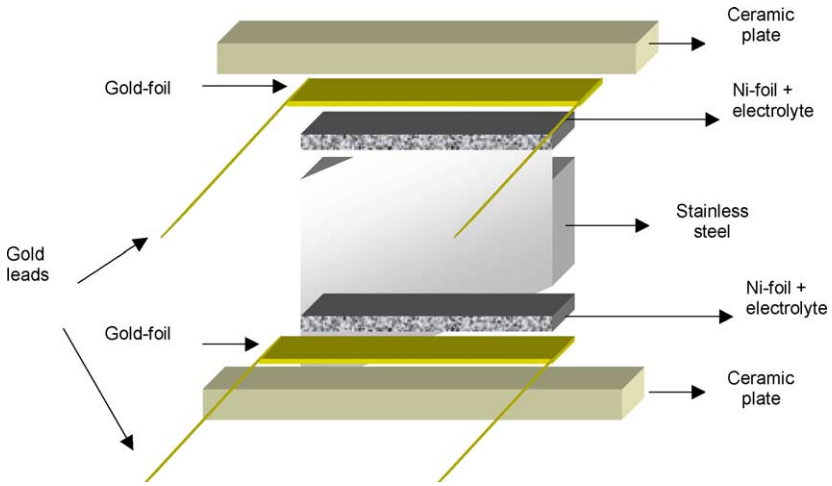


Fig. 2. Schematic of the sample arrangement for the electrical resistivity test.

## 3. Results

### 3.1. Results of the corrosion tests

The obtained oxide layer thickness on the investigated hot rolled steels after 340, 650, 3000 and 5000 h of exposure is shown in Fig. 3.

The corrosion scales developed on Alloy V 152 (12.2% Mn) after 340 and 5000 h of exposure are shown in Fig. 4(a and b). The oxide scale formed after 340 h is only a few microns thick but already shows a multilayer structure. The outer layer in contact with melt is mainly (Li, Fe) oxide with some Mn in solid solution, whereas chromium is present as soluble $K_2CrO_4$. On the metal side, the chromium-rich spinel oxide also containing Mn is formed and in between this and the outer layer, a chromium-free (Fe, Co) spinel, with significant amounts of Mn is detected. After 3000 and 5000 h, the multilayer structure is more dominant due to an outward diffusion of manganese. Hence, in the outer part an enrichment of Mn occurs while the intermediate layer is now (Fe, Cr) spinel oxide with dissolved Mn. The chromium-rich oxide remains in contact with the metal and some dissolved Fe, Mn, Mo and Co are present.

After 340 h the corrosion scale on Alloy V 155 (9.75% Co) consists of three layers as seen in Fig. 5(a). On the surface, $K_2CrO_4$ has formed like in the case of alloy V 152, as well as (Li, Fe) oxide without any Co. The middle layer is $FeCr_2O_4$ with dissolved Co and Mn, whereas the inner layer consists of (Fe, Cr) spinel oxide with dissolved Mn, Ni and Mo. After 5000 h of exposure, Ni diffuses outwards and the overall scale is enriched in nickel (Fig. 5(b)). Compared to the alloy V 152, with a lower Co-content, the outward diffusion of

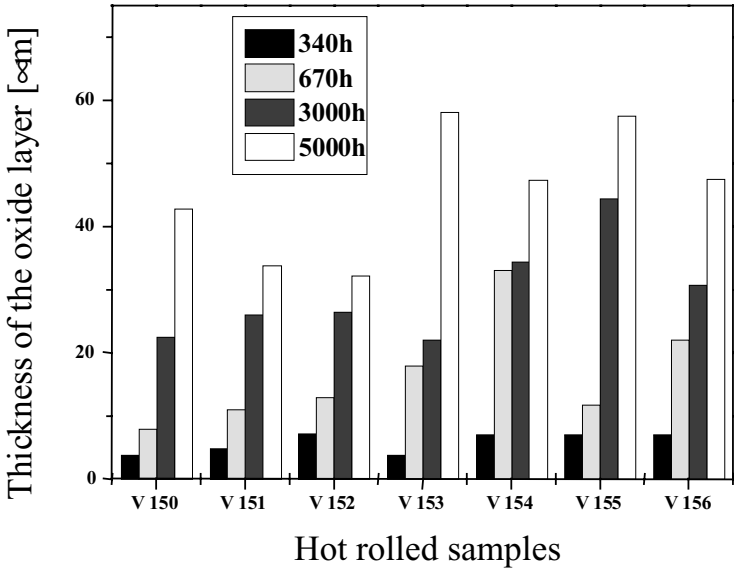


Fig. 3. Oxide scale thickness as a function of time.

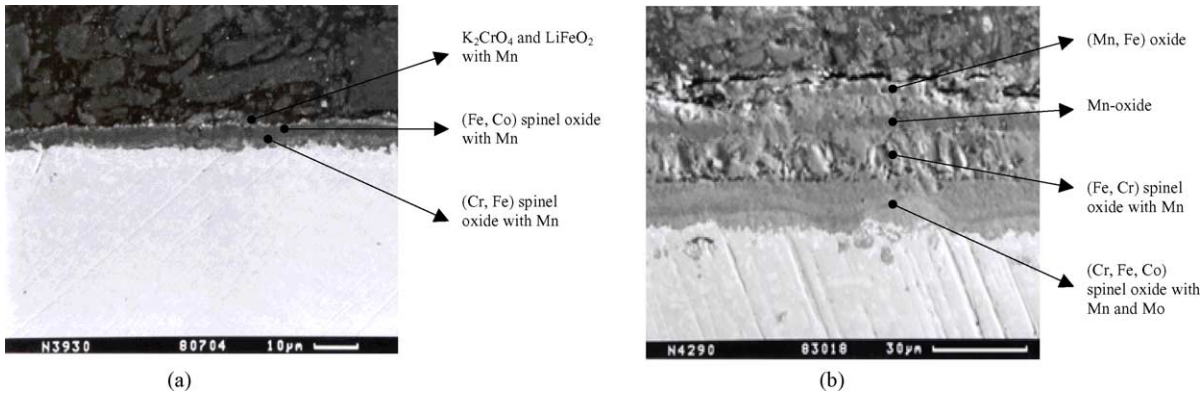


Fig. 4. Corrosion scales on alloy V 152 after different exposure times: (a) 340 h, (b) 5000 h.

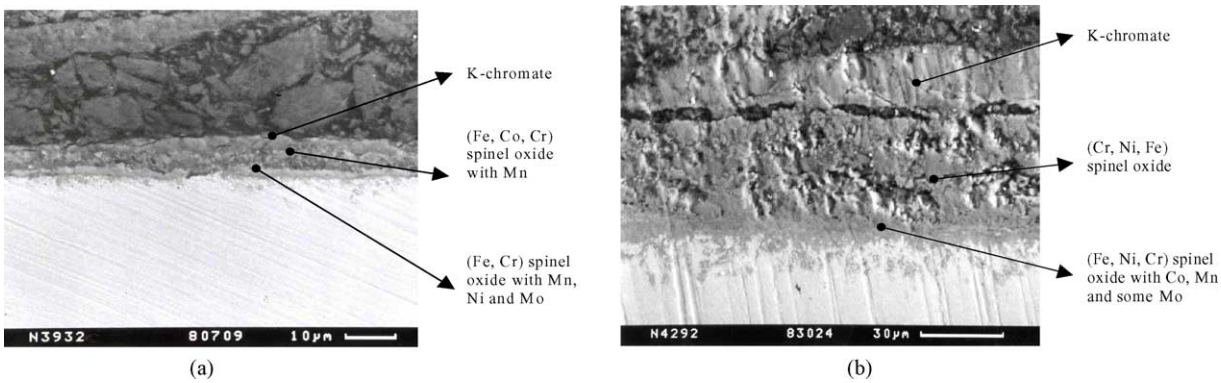


Fig. 5. Corrosion scales on alloy V 155 after different exposure times: (a) 340 h and (b) 5000 h.

Mn, Co and Mo is suppressed, which is beneficial for the electronic conductivity. However, the high Ni content, up to 14 wt.%, increases the corrosion resistivity of Fe–18% Cr alloys since no breakaway Fe–Cr spinels are formed locally [5].

The formation of $LiFeO_2$ with some dissolved Co and $K_2CrO_4$, on a top of the scale on Alloy V 151 (1.98% Mn) is confirmed by SNMS depth profile measurement (Fig. 6).

The inner layer is (Cr, Ni) spinel oxide with Mn and Mo (Fig. 7(a)). During longer exposure times (5000 h, Fig. 7(b)),

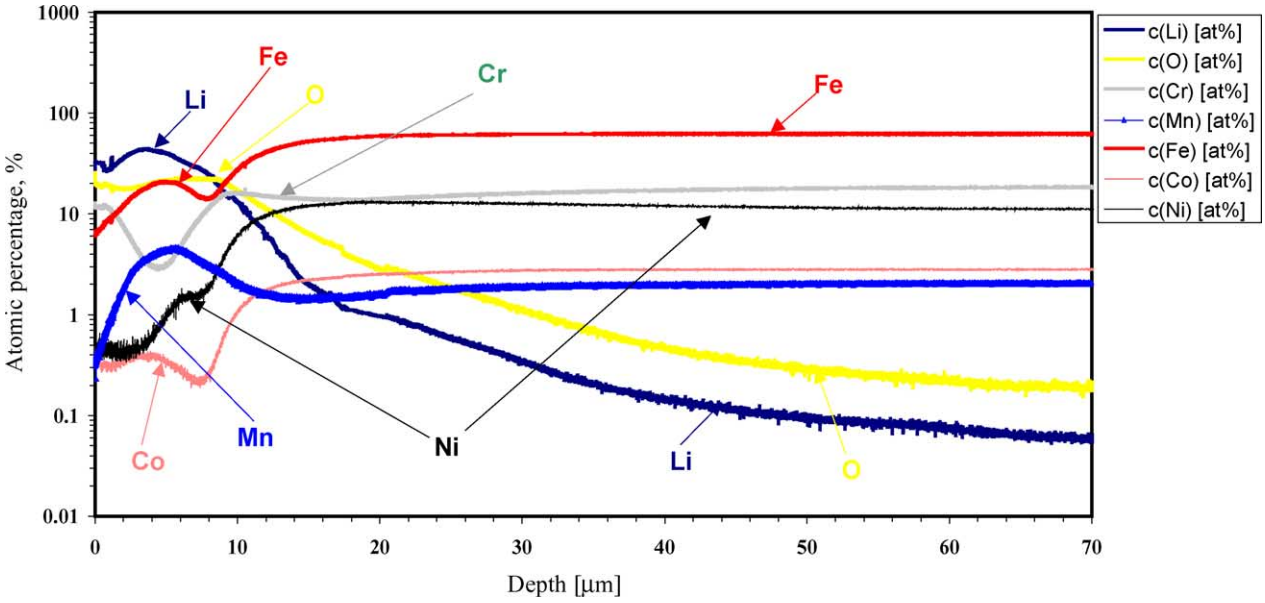


Fig. 6. SNMS depth profile of alloy V 151 after 5000 h of exposure.

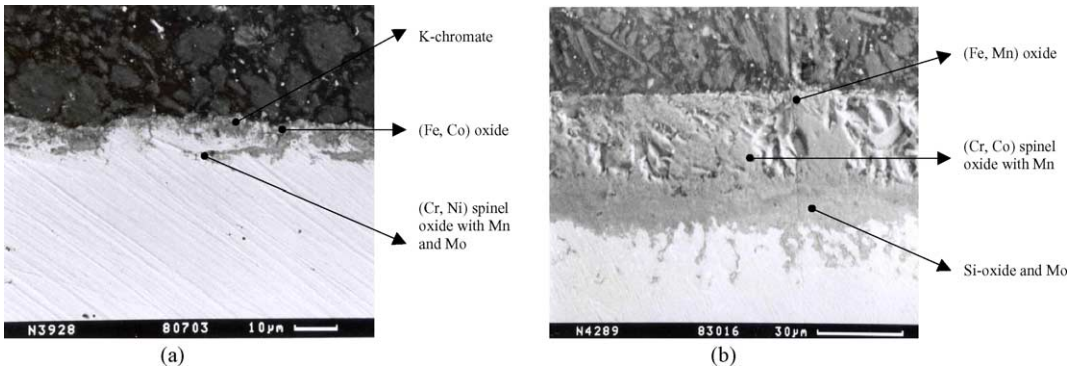


Fig. 7. Corrosion scales on alloy V 151 after different exposure times: (a) 340 h and (b) 5000 h.

Mn and Fe diffuse outwards and an intermediate layer of (Cr, Co) spinel oxide with some Mn is formed. Silicon-oxide is detected at the metal/oxide interface. The oxide scale formed on the alloy is compact and dense and, therefore, improve the corrosion protection.

All investigated alloys have a similar amount of Cr and Si except Alloy V 154 with the lowest content of Si (0.0226 wt.%). The corrosion scales formed on this alloy are shown in Fig. 8(a and b). After 340 h of exposure (Fig. 8(a)) the outer oxide layer is (Li, Fe) oxide with dissolved Mn and a small amount of $K_2CrO_4$. (Fe, Cr) spinel oxide with dissolved Mn forms as an intermediate layer and the complex (Fe, Cr, Ni) oxide of spinel type with Mn, Mo and Co is formed in contact with the metal. After 5000 h (Fig. 8(b)), Co diffuses outward by forming the outer oxide layer of (Li, Fe) oxide with Mn and Co in solid solution. However, no Co was detected in the intermediate layer. The inner part of the scale consists of (Cr, Fe) spinel oxide which contains dissolved Mn and some Co and Mo. With increasing reaction time, Co and Mn diffuse further outwards, like already observed for Mn on Alloy 152. The morphology of the oxide layer exhibits a lot of cracks, obviously due to a lower Si-content in this alloy.

### 3.2. Electrical resistivity measurements

The electrical resistivities of the different investigated stainless steels are shown as a function of time in Fig. 9.

Alloy AC 66 has a resistivity in the range of 65–437 mΩ cm$^2$ after 700 h. This value is higher than acceptable for steels as CCC in MCFC (about 50–150 mΩ cm$^2$), accordingly, the corrosion resistance of this alloy is rather good (14 μm after 700 h). The thickness of the corrosion layer of 1.4404 steel currently used as CCC after 700 h is 15 μm [6]. In Fig. 10(a and b) cross-section SEM pictures of AC 66 after different exposure times in simulated MCFC conditions are presented.

After 280 h the large increase in the resistivity of AC 66 is due to the formation of a low conductive Cr-rich oxide, but also the outer porous Fe-oxide scale with cracks increases the overall resistivity. With increased exposure time, 700 h, the resistivity decreases and SEM photo in Fig. 10(b) shows the formation of two layers: the outer (Li, Fe) oxide with a small amount of Mn and the inner (Fe, Ni)$Cr_2O_4$ layer. This inner spinel layer has a better conductivity than a pure $LiCrO_2$ and additionally, the Mn present in the outer oxide increases the conductivity [7] as well. Hence, this alloy shows a bad electronic conductivity due to the high content of Cr (27.8 wt.%).

A lower resistivity of alloy Alloy V 150 compared to AC 66 is mainly due to a lower content of Cr which promotes the formation of spinels with a better conductivity due to a replacement of Cr ions by Mn, Ni and Co. The oxide formed in contact with the melt is (Li, Fe) oxide with a small amount of dissolved Co and also some K-chromate

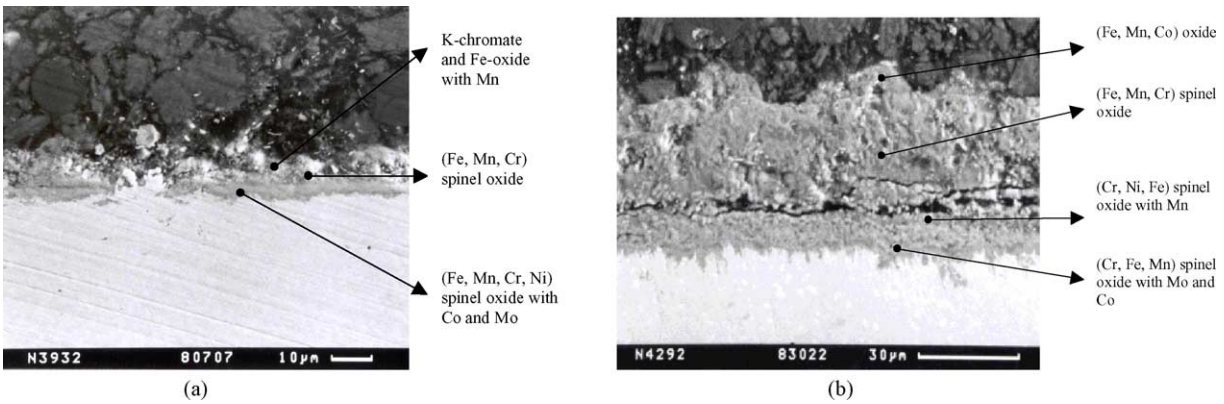


Fig. 8. Corrosion scales on alloy V 154 after different exposure times: (a) 340 h and (b) 5000 h.

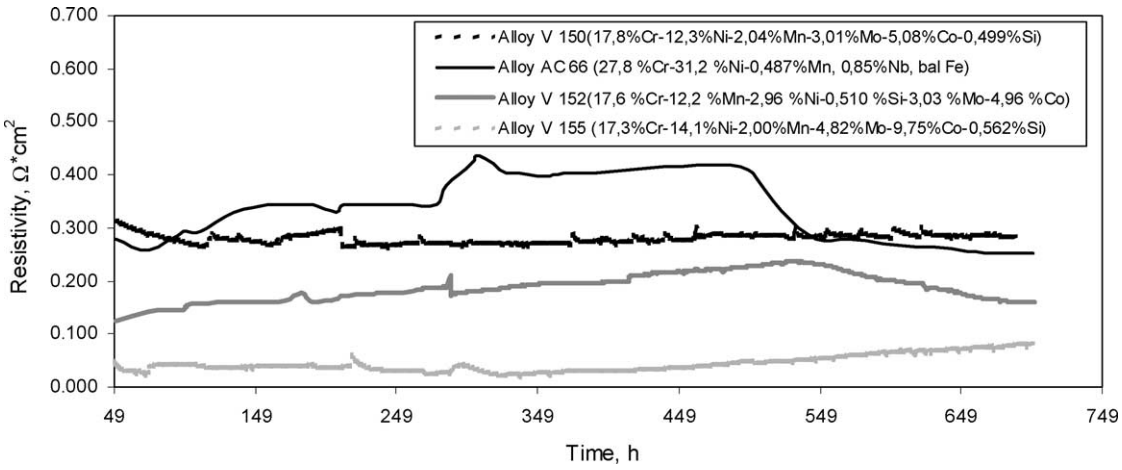


Fig. 9. Electrical resistivities of the different investigated alloys.

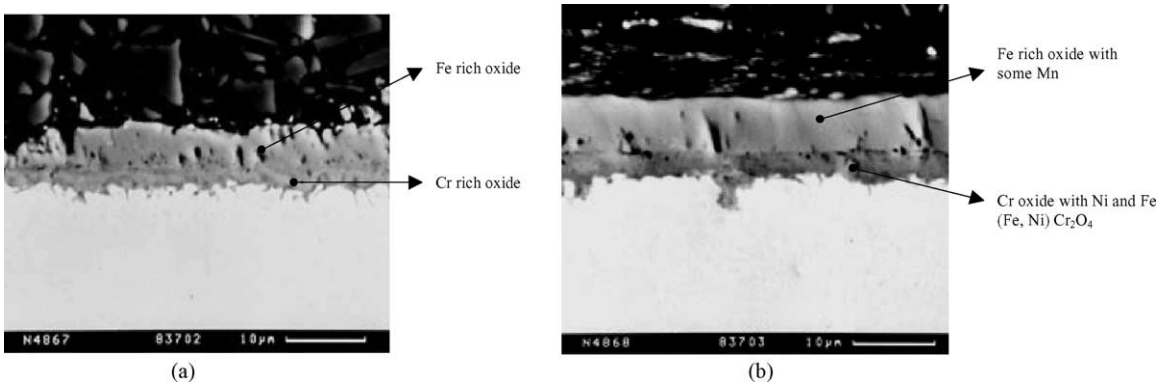


Fig. 10. Corrosion scales on alloy AC 66 after different exposure times: (a) 280 h and (b) 700 h.

on top of the scale (Fig. 11(a)). The intermediate layer is a (Cr, Fe, Ni) spinel oxide with some dissolved Mn and the layer on the steel side is (Cr, Fe, Ni) spinel oxide with Mo and some Si-oxide. The same distribution of the elements was observed after 700 h (Fig. 11(b)), some differences in the composition of the outer layer were detected due to the outwards diffusion of Ni and Mn.

Alloy V 152 has a conductivity values between those of V 150 and V 155. The Mn content in this alloy is 12.2 wt.% which should assure the formation of the Mn-containing spinels with a good conductivity in the inner parts of the formed oxide scale, confirming the positive effect of Mn on the conductivity [8]. SEM analysis of samples after 300 and 700 h is shown in Fig. 12(a and b).

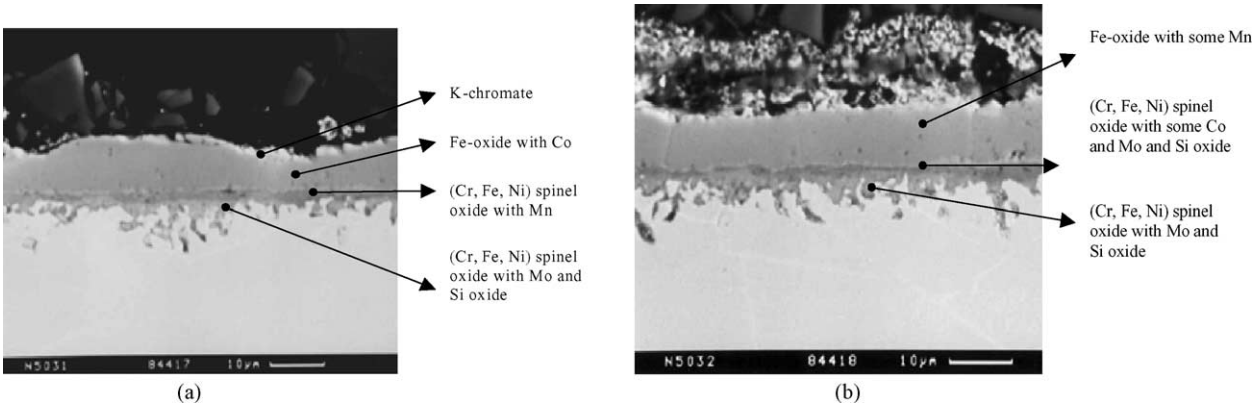


Fig. 11. Corrosion scales on alloy V 150 after different exposure times:(a) 450 h and (b) 700 h.

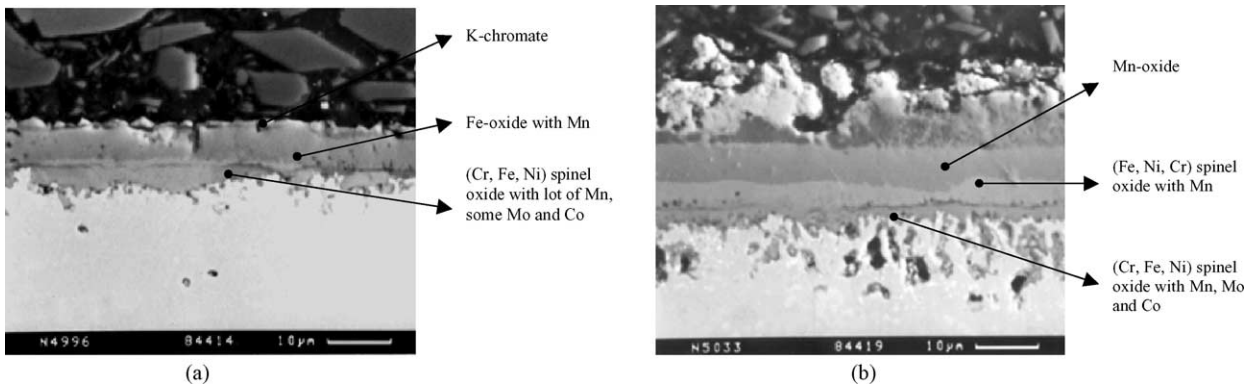


Fig. 12. Corrosion scales on alloy V 152 after different exposure times (a) 300 h and (b) 700 h.

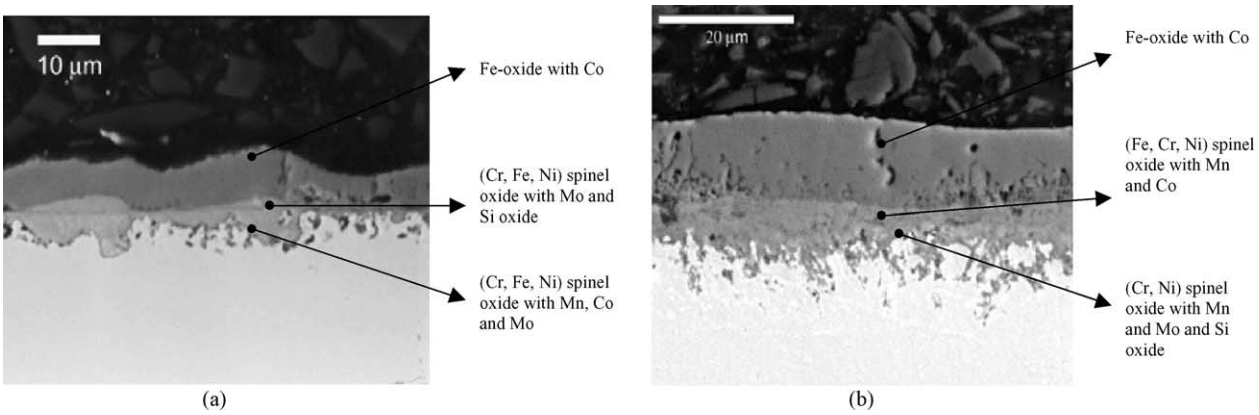


Fig. 13. Corrosion scales on alloy V 155 after different exposure times: (a) 100 h and (b) 700 h.

After 300 h (Fig. 12(a)), the (Li,Mn) containing oxide is present in the outer part of a scale. The Co concentration in the steel is low (2.98 wt.%) and, therefore, the formation of $LiCoO_2$ with low resistivity [9] is unlikely. With increasing time (700 h, Fig. 12(b)), the resistivity of this alloy decreases due to the formation of an inner spinel layer with a higher content of Mn and less Cr. Comparing the two alloys, V 150 and V 152, with significant differences in Mn and Ni content and a small difference in the other alloying elements (Co, Mo, Si), one can conclude that, relative to Ni, Mn promotes much more the formation of layers with a better conductivity.

Alloy V 155 exhibits the best conductivity (after 700 h in a range of 20–80 $m\Omega\,cm^2$). The oxide scales after different exposure times are shown in Fig. 13(a and b). The highest content of Mo and Ni in this alloy and also the high Co content appeared to be beneficial for the conductivity of the oxide scale. After 100 and 700 h of exposure a three-layered scale is formed with Co containing (Li, Fe)-oxide as an outer and (Fe, Cr, Ni) spinel oxides, with dissolved Mn, Co and Mo as an inner layer. Not only the presence of mentioned elements but also a high Fe content in these spinels is responsible for the low resistivity [10].

## 4. Discussion

Since the spinel oxide layers, formed as intermediate and inner layers of the oxide scale seems to have the major influence on the conductivity and the corrosion resistance of the tested alloys, further investigations of inner oxide scale on V 150, V 152 and V 155 alloys were carried out.

The reaction of spinel formation can be written in terms of a solid state reaction as:

$$AX + B_2X_3 = AB_2X_4 \quad (2)$$

where A and B are cations and X anion. A formed spinel $AB_2X_4$, generally, can be considered as a ternary crystal which consists of one phase and three components. For defining the thermodynamic state of this crystal four state variables must be fixed, according to the phase rule. Apart $T$, $P$ and $p_{O_2}$, which were variables used for a long time to obtain the diffusion data, *Schmalzried* introduced an activity of one oxide component $a_{AX}$ as a fourth variable [11]. With a use of the following assumptions: (a) the oxides under consideration are of theoretical density; (b) electroneutrality is maintained; (c) nonequilibrium defects, like grain boundaries and dislocations, do not influence the spinel formation rates, the spinel growth rate will be diffusion controlled,

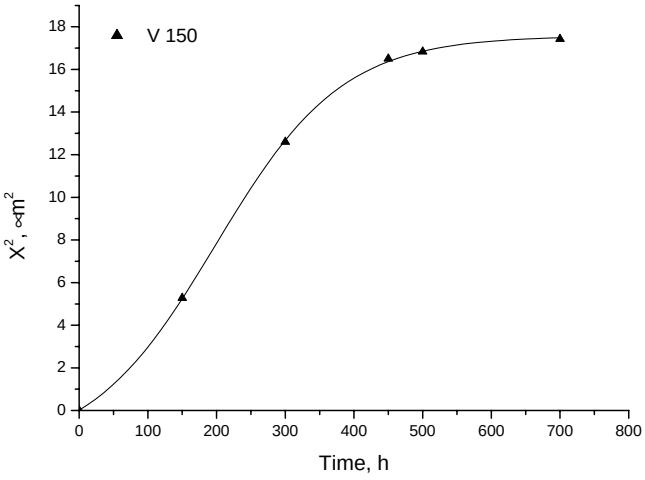


Fig. 14. Inner scale thickness of alloy V 150 as a function of time at 650 °C.

since the chemical reaction is rapid in comparison with the transport through the oxide. There are five suggested mechanisms of spinel growth (X is $O^{2-}$): (1) diffusion of doubly ionised cations and anions through the spinel layer and reaction at the $B_2O_3$ interface, (2) divalent cations and electrons diffusion through the spinel layers, while oxygen follows a short-circuit path through the gas phase, (3) and (4) are analogous to (1) and (2) but reaction occurs on side of AO oxide and mechanism (5) called Wagner mechanism, represents inverse cation diffusion through the spinel layer [12]. In the case of an alloy, containing more than two elements the spinel composition is not stable with time and diffusion of elements occur, like observed for Co, Mn and also Ni. For that reason and in accordance with the Schmalzried model the thermodynamic state of the spinel phase is changing continuously during exposure and the diffusion of species gradually changes. Hence, the growth rate of the spinel phase must be depending on time.

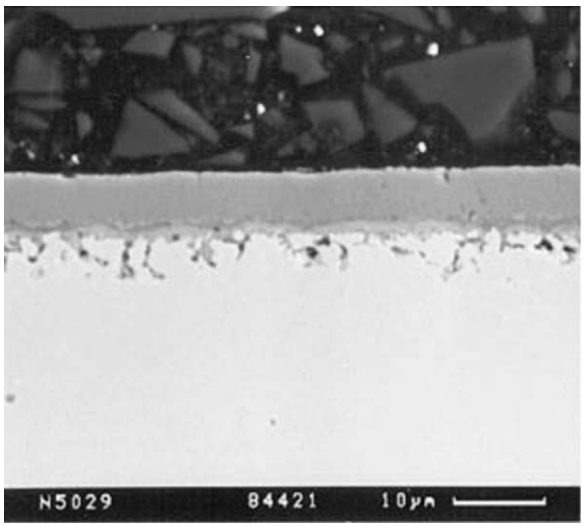


Fig. 15. SEM cross-section of alloy V 150 after 120 h of exposure.

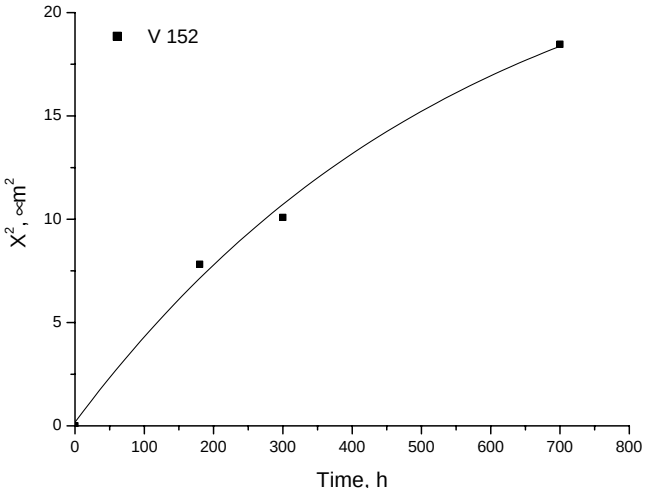


Fig. 16. Inner scale thickness of alloy V 152 as a function of time at 650 °C.

If diffusion controlled, the rate of spinel layer growth will be inversely proportional to its thickness:

$$\Delta x^2 = 2k_p t \quad (3)$$

where is $k_p$ the parabolic rate constant for the formation of a spinel layer of thickness $\Delta x$ during time $t$. The careful measurements of the inner scale depth $X$, obtained from the SEM photos, are used to plot diagrams $X^2$ versus time. For the alloy V 150 such a diagram is presented in Fig. 14.

After the first 100 h of exposure at 650 °C the curve is almost linear (Fig. 14). A cross-section SEM photo of the alloy after 120 h (Fig. 15) shows the inner layer of a (Fe, Cr) spinel oxide with some dissolved Mo. Between 100 and 400 h the oxidation rate slightly increases, this can be explained with a Ni diffusion in this spinel and replacement of some Cr by Ni. The second change in the oxidation rate occurred after 450 h and in the inner layer Si-oxide is detected by EDX. The decrease of oxidation rate in Fig. 14

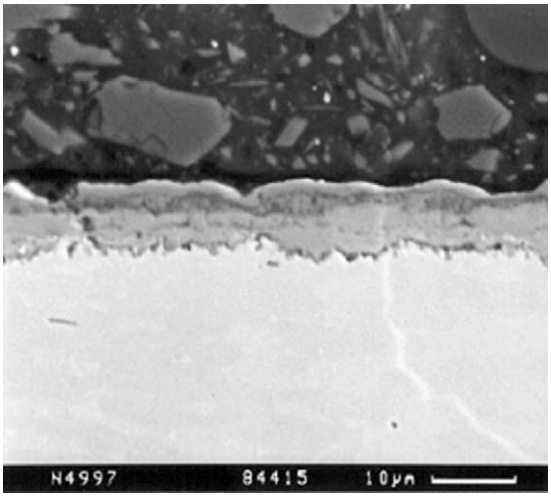


Fig. 17. SEM cross-section of alloy V 152 after 180 h of exposure.

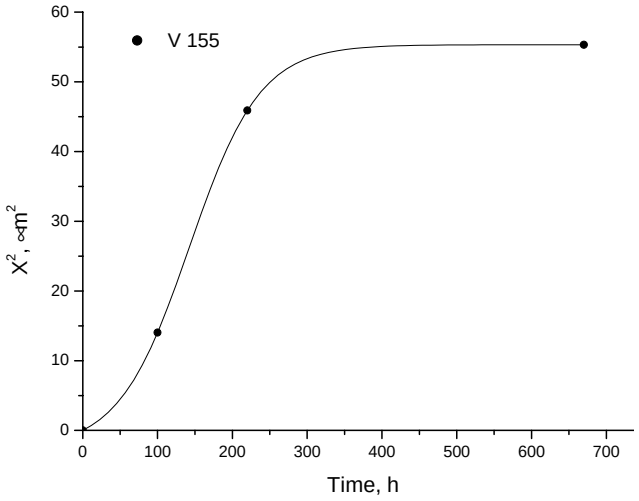


Fig. 18. Inner scale thickness of alloy V 155 as a function of time at 650 °C.

is understandable since Si-oxide is known to be slow growing.

The inner scale growth of alloy V 152 shows different behaviour (Fig. 16). In the first 700 h a continuous increase of the inner oxide scale thickness was observed, however, after 5000 h this alloy has the thinnest oxide scale (Fig. 3). The resistivity increases in the first 500 h (Fig. 9) and than drops down. After 300 h a change of slope in Fig. 16 can be seen and as already seen in Fig. 12(a), after 300 h of oxidation, an inner (Cr, Fe, Ni) spinel rich in Mn has formed, slightly changing the activity of species in the oxide and, therefore, its growth rate. With time, the Mn content increases, leading to a decreased resistivity. SEM cross-section of oxide scale on alloy V 152 after 180 h of exposure is shown in Fig. 17.

The inner oxide growth of alloy V 155 in the first 200 h is faster than observed for V 150 and V 152, however, subsequently decreasing with time (Fig. 18). From Fig. 9, it can be seen that after this time resistivity increases. This suggests that fast growing inner spinel oxides, with Mn, Co or Ni ions incorporated and formed in the first 200 h, shows a good electronic conductivity. The change in the oxidation rate and resistivity as well occurs due to the presence of Si oxide in the inner layer of the scale after longer time Fig. 13(a and b). The change in the resistivity can be also explained with an outward diffusion of Co and Mn and more Cr present in the inner spinel layer, which decrease a conductivity of spinel. A porous inner oxide layer is already present in the first 200 h of oxidation (Fig. 19) and this also has a beneficial effect on the oxide growth.

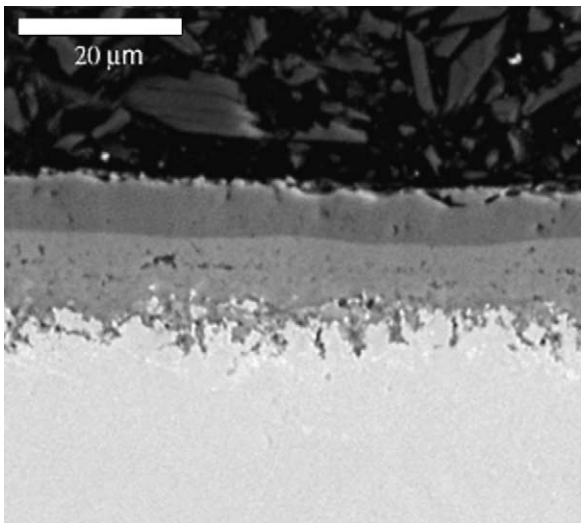


Fig. 19. SEM cross-section of alloy V 155 after 220 h of exposure.

An absence of the linear dependence in Figs. 14, 16 and 18 can possibly be attributed to the fact that these observed spinels are not “pure” but (Fe, Cr) spinel oxide with Mn, Co, Ni and Mo, or (Cr, Co) spinels with Mn, Ni and Mo, or (Cr, Ni) spinels with Co, Mn, Mo in solid solution. It seems that the parabolic law cannot be applied completely to these complex oxide systems without a certain corrections.

## 5. Conclusions

The corrosion and the resistivity tests have shown that under MCFC cathodic conditions the investigated alloys form a multilayer oxide scales with an outer $LiFeO_2$ with Mn and Co in solid solution and $K_2CrO_4$, in contact with the melt. Furthermore, inner spinel oxide layers, $(Fe, Cr, Ni)_3O_4$ with Mn, Co and Mo in solid solution, variable in composition as a function of time and also from the metal/scale interface to the spinel/ferrate interface. With time, Mn and Co diffuse outwards and Mo preferably stays at the metal side. The investigations on the oxide penetration depth showed a close correlation between the nature of the inner spinels and the resistivity of the alloys. The best corrosion resistance after longer times (5000 h) has alloy V 152 with the highest Mn content (12.2%) but in a shorter time (700 h) the inner oxidation zone in this alloy increases without showing a plateau in $X^2$ versus time plot. This is attributed to the less Cr concentration in the inner layer, in combination with more Mn, which increases the conductivity. The highest electrical conductivity has alloy V 155 with the highest Ni and Mo content (14.1% Ni and 4.82% Mo) and high Co content (9.75%). The nature of an inner spinel is brought in connection with the conductivity and the corrosion resistance. Conductivity decrease coincidence with the formation of an inner spinel oxide, diluted with Fe, Mn and Co. An enrichment of this spinel with Cr leads to a lower inner oxidation rate. The composition of the inner oxide layer influence a lot the overall oxidation behaviour as well as the conductivity of the alloy. It seems that Mn, Co and Ni are the most significant elements for the formation of a good conductive oxide scale while Si and Cr are responsible for a good corrosion resistance.

## References

[1] A.C. Schoeler, T.D. Kaun, M. Krumpelt, Influence of the alloying elements Man and Co on the electrical resistance and corrosion behaviour of bipolar plate materials in MCFC, Electrochem. Soc. Proc. 99–20 (1999) 158–168.
[2] K.A. Hay, F.G. Hicks, D.R. Holmes, The transport properties and defect structure of the oxide (Fe, $Cr)_2O_3$ formed on Fe–Cr alloys, Werkstoffe Korr. 11 (1970) 917–924.
[3] F.A. Kröger, The Chemistry of Imperfect Crystals, North-Holland Publishing Company, Amsterdam, Netherlands, 1964, p. 733.
[4] G. Feuillade, R. Coffre, G. Outhier, Emploi des oxydes métalliques 3d et 4d comme catalyseurs dans les piles oxygéne–hydrogéne, Ann. Radioelectr. 21 (1966) 105–121.
[5] W.B. Sharp, Incorporation of divalent cations in $Cr_2O_3$ during the oxidation of Fe–18% Cr–Ni alloys at 1123 K, Corros. Sci. 10 (1970) 283–295.
[6] P. Biedenkopf, T. Wochner, High temperature materials in molten carbonate fuel cells, in: High Temperature Material Chemistry Proceedings of the 10th International IUPAC Conference, Part I, 2000, pp. 707–710.
[7] L. Plomp, J.B.J. Veldhuis, E.F. Sitters, S.B. van der Molen, Improvement of molten carbonate fuel cell (MCFC) lifetime, J. Power Sources 39 (3) (1992) 369–373.
[8] F.A. Kröger, The Chemistry of Imperfect Crystals, North-Holland Publishing Company, Amsterdam, Netherlands, 1964, p. 737.
[9] I. Bloom, M.T. Lanagan, M. Krumpelt, J.L. Smith, The development of $LiFeO_2$–$LiCoO_2$–NiO cathodes for molten carbonate fuel cells, J. Electrochem. Soc. 146 (4) (1999) 1336–1340.
[10] T.D. Kaun, A.C. Schoeler, I. Bloom, M. Lanagan, M. Krumpelt, Resistivity of bipolar plate materials at the cathode interface in molten carbonate fuel cells, Presented at the 194th Meeting of the Electrochemical Society, Boston, MA, USA, 1998.
[11] H. Schmalzried, Point defects in ternary ionic crystals, Prog. Chem. Solid State 2 (1965) 265–303.
[12] J.S. Armijo, The kinetics and mechanism of solid-state spinel formation—a review and critique, Oxid. Met. 1 (2) (1969) 171–198.